X-ray Crystal Structures of *Moorella thermoacetica* FprA. Novel Diiron Site Structure and Mechanistic Insights into a Scavenging Nitric Oxide Reductase[†,‡]

Radu Silaghi-Dumitrescu,[§] Donald M. Kurtz, Jr.,[§] Lars G. Ljungdahl,[||] and William N. Lanzilotta*,[||]

Department of Biochemistry and Molecular Biology, Department of Chemistry, and Center for Metalloenzyme Studies, University of Georgia, Athens, Georgia 30602

Received December 22, 2004; Revised Manuscript Received March 7, 2005

ABSTRACT: Several members of a widespread class of bacterial and archaeal metalloflavoproteins, called FprA, likely function as scavenging nitric oxide reductases (S-NORs). However, the only published X-ray crystal structure of an FprA is for a protein characterized as a *r*ubredoxin:di*o*xygen *o*xidoreductase (ROO) from *Desulfovibrio gigas*. Therefore, the crystal structure of *Moorella thermoacetica* FprA, which has been established to function as an S-NOR, was solved in three different states: as isolated, reduced, and reduced, NO-reacted. As is the case for *D. gigas* ROO, the *M. thermoacetica* FprA contains a solvent-bridged non-heme, non-sulfur diiron site with five-coordinate iron centers bridged by an aspartate, and terminal glutamate, aspartate, and histidine ligands. However, the *M. thermoacetica* FprA diiron site showed four His ligands, two to each iron, in all three states, whereas the *D. gigas* ROO diiron site was reported to contain only three His ligands, even though the fourth His residue is conserved. The Fe1−Fe2 distance within the diiron site of *M. thermoacetica* FprA remained at 3.2−3.4 Å with little or no movement of the protein ligands in the three different states and with conservation of the two proximal open coordination sites. Molecular modeling indicated that each open coordination site can accommodate an end-on NO. This relatively rigid and symmetrical diiron site structure is consistent with formation of a diferrous dinitrosyl as the committed catalytic intermediate leading to formation of N_2O. These results provide new insight into the structural features that fine-tune biological non-heme diiron sites for dioxygen activation vs nitric oxide reduction.

A widespread class of bacterial and archaeal proteins called FprA[1] (or A-type flavoprotein) contain a metallo-β-lactamase-like domain immediately followed in the amino acid sequence by a flavodoxin-like domain (*1*, *2*). The only published X-ray crystal structure of an FprA is for a protein named *r*ubredoxin:*o*xygen *o*xidoreductase (ROO), isolated from the anaerobic sulfate-reducing bacterium *Desulfovibrio gigas* (*3*). The *D. gigas* ROO structure showed a unique active site featuring an FMN across the homodimeric subunit interface from a non-heme, non-sulfur diiron site, as shown in Scheme 1.

Scheme 1

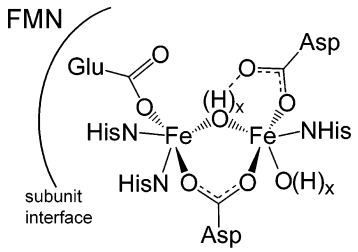

These two prosthetic groups were contributed from the flavodoxin-like and metallo-β-lactamase-like domains, respectively. The diiron site was ligated by histidine, glutamate, and aspartate side chains and appeared to have a bridging solvent ligand but otherwise bore no apparent relationship to those in other diiron proteins. A lactam binding region was also not apparent. The *Escherichia coli* FprA homologue was named flavorubredoxin because of an extra rubredoxin-type domain at its C-terminus (*4*). Flavorubredoxin nevertheless contains the metallo-β-lactamase and flavodoxin domains in the respective N- to C-terminal order that define the FprA class.

As its name implies, in vitro evidence indicated that the *D. gigas* ROO functioned as a dioxygen reductase (O_2R), catalyzing the four-electron reduction of dioxygen to water (*5*, *6*). More recent genetic and biochemical evidence, however, indicates that many bacterial FprAs, including those from *E. coli* (*7*, *8*), *Moorella thermoacetica* (*9*), *Desulfovibrio vulgaris* (*10*), and *Salmonella enterica* (*11*), function *in vivo* as the terminal component of a nitric oxide reductase (NOR).

[†] This work was supported by NIH Grant GM40388 (to D.M.K.).

[‡] Atomic coordinates have been deposited in the Protein Data Bank. The accession numbers are 1YCF, 1YCG, and 1YCH.

* To whom correspondence should be addressed at the Department of Biochemistry and Molecular Biology. Phone: 706-542-1324. Fax: 706-542-1738. E-mail: wlanzilo@bmbiris.bmb.uga.edu.

[§] Department of Chemistry and Center for Metalloenzyme Studies.

[||] Department of Biochemistry and Molecular Biology and Center for Metalloenzyme Studies.

[1] Abbreviations: FprA, flavodiiron protein; NOR, nitric oxide reductase; S-NOR, scavenging nitric oxide reductase; O_2R, dioxygen reductase (four-electron reduction of dioxygen to water); ROO, rubredoxin:oxygen oxidoreductase; Hrb, high molecular weight rubredoxin (NADH:FprA oxidoreductase); MOPS, *N*-morpholinoethanesulfonic acid; IPTG, isopropyl β-D-thiogalactoside; FMN, oxidized flavin mononucleotide; $FMNH_2$, fully reduced flavin mononucleotide; PEG, poly(ethylene glycol); DEA-NONOate, diethylamine NONOate sodium salt (Sigma Chemical Co., St. Louis, MO).

10.1021/bi0473049 CCC: $30.25
Published on Web 04/08/2005

Scheme 2

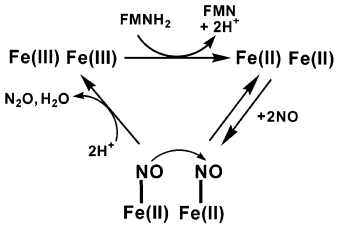

These soluble, cytoplasmic FprAs are distinct from the membrane-bound respiratory NORs characteristic of denitrifying bacteria (*12*, *13*). The denitrifying NORs and the aforementioned FprAs both catalyze the electron donor:nitric oxide oxidoreductase reaction:

$$2e^- + 2H^+ + 2NO \rightarrow N_2O + H_2O \qquad (1)$$

The NOR activity of FprA, however, is not energy conserving; it rather serves a scavenging function, protecting against "nitrosative stress", which can occur either as a consequence of nitrate metabolism or as a host response to infection or colonization (*14*−*16*). We, therefore, define this activity as scavenging nitric oxide reductase (S-NOR) but retain the FprA designation for this class of proteins, since it is not yet clear whether all such homologues function as NORs (vide infra). In the case of *M. thermoacetica* FprAs, the reducing equivalents in eq 1 are donated by NADH via a flavoiron reductase referred to as high molecular weight rubredoxin (Hrb) (*9*). A mechanism for S-NOR catalysis that is consistent with our analysis of the steady-state kinetics for *M. thermoacetica* (*9*) and *D. vulgaris* (*10*) FprAs is shown in Scheme 2. According to this scheme, the rate-determining step in turnover (i.e., k_{cat}) at saturating Hrb and NADH occurs following preequilibrium, cooperative binding of two NOs by the diferrous site, forming a diferrous dinitrosyl intermediate.

The generality of the NOR activity for FprAs, however, has been questioned (*17*, *18*). The *D. gigas* ROO, for example, has not been reported to show NOR activity, whereas the *E. coli*, *M. thermoacetica*, and *D. vulgaris* FprAs show both NOR and O_2R activities *in vitro* (*4*, *9*, *10*, *19*). While the anaerobic NOR activity of these latter three FprAs is relatively robust, their aerobic O_2R turnover results in irreversible inactivation.

M. thermoacetica (formerly *Clostridium thermoaceticum*) is a Gram-positive bacterium classified as a strict anaerobe; it has served as the prototypical acetogen and can grow autotrophically on CO_2 and H_2 (*20*). However, when given a choice, *M. thermoacetica* preferentially utilizes dissimilatory nitrate reduction for growth (*21*), which is consistent with an S-NOR role for its FprA. In an attempt to correlate structural differences with organismic origin and the apparent NOR/O_2R dichotomy, we solved the crystal structure of the *M. thermoacetica* FprA previously characterized by us (*9*). Comparison with the crystal structure of the *D. gigas* ROO (*3*) reveals conserved features as well as a significant difference between the diiron sites. Crystal structures are reported for the oxidized ("as-isolated"), reduced, and reduced, NO-reacted *M. thermoacetica* FprA. The implications of the crystallographic results for the mechanism of NO reduction at the FprA active site and possible reasons for the apparently differing catalytic activity of *D. gigas* ROO are discussed.

MATERIALS AND METHODS

Reagents and General Procedures. All solutions were prepared in deionized water. NADH, NADPH, PEG (Sigma Chemical Co.), and DEA NONOate [diethylammonium (*Z*)-1-(*N*,*N*-diethylamino)diazen-1-ium-1,2-diolate; Cayman Chemicals, Inc.] were used without further purification. All protein concentrations are expressed in monomers. Recombinant *M. thermoacetica* FprA and Hrb were obtained as previously described and used without further purification (*9*). UV−vis absorption spectra of FprA crystals were recorded in melting point capillaries using a QDI1000 UV−vis−NIR microspectrophotometer (Craic Technologies, Inc.). Other absorption measurements were obtained on a Shimadzu UV2010PC spectrophotometer.

FprA Crystallization. FprA solutions used for crystallization were ∼1 mM in monomer [determined using a published extinction coefficient (*9*)] in 25 mM MOPS, pH 7.3. Preliminary screenings were performed using both sitting drop and batch methods with the following commercial reagent sets: Wizard I, Wizard II (Decode, Inc.), Crystal Screen 1, Crystal-Screen 2, Peg-Ion Screen, and MembFac (Hampton Research). The crystals eventually used for data collection were obtained from batch crystallization in melting point capillaries at room temperature by layering 10 μL of the precipitant (200 mM zinc acetate, 50 mM sodium cacodylate, pH 6.5, 5% 2-propanol) with 10 μL of the oxidized (as-isolated) FprA solution. Diffraction quality crystals typically formed within 7−10 days. Similar crystals were obtained using a slightly different precipitant: 200 mM zinc acetate, 100 mM sodium acetate, pH 4.5, and 10% PEG 3000. FprA crystals obtained as described above suffered visible damage when flash-frozen either by dipping into liquid nitrogen or by sudden exposure to a stream of nitrogen gas cooled to −185 °C. Ethylene glycol was, therefore, employed as cryoprotectant. To this end, crystals were progressively soaked for ∼20 min in mother liquor [i.e., 1:1 (v/v) 25 mM MOPS (pH 7.3):precipitant] containing ethylene glycol in 5% increments, up to 20%.

Anaerobic solutions of reduced FprA for crystallization screening were generated inside a gloved anaerobic chamber (Coy Laboratory Products, Inc.) with an atmosphere containing 85% N_2, 10% CO_2, 5% H_2, and routinely <1 ppm O_2. Reduction was readily achieved at room temperature inside the anaerobic chamber by adding a few crystals of sodium dithionite to ethylene glycol-treated, as-isolated FprA crystals that were sitting in a well of a 9-well glass plate containing 200 μL of mother liquor [containing the pH 6.5 precipitant and 20% (v/v) ethylene glycol]. Upon treatment with dithionite, the FprA crystals changed within a few minutes from orange-brown to colorless.

For reaction with NO, the dithionite-reduced FprA crystals in the anaerobic chamber were soaked for 20 min in anaerobic dithionite-free mother liquor [containing the pH 6.5 precipitant and 20% (v/v) ethylene glycol] and then treated with a few grains of the NO-releasing agent, DEA-NONOate, at room temperature. This treatment resulted in rapid reoxidation of the crystalline FprA, manifested as a change in color from clear to orange-brown. These reduced

and reduced plus NO-treated FprA crystals, maintained under the anaerobic mother liquor on a tape-covered glass plate, were removed from the anaerobic chamber, mounted on loops, and flash-frozen by dipping in liquid nitrogen. The time elapsed between removing the crystals from the anaerobic chamber to flash-freezing was approximately 40 s, and the crystals were at all times covered in mother liquor containing either excess sodium dithionite or NO (from the DEA NONOate). For the latter crystals, a 1 h soak in anaerobic dithinoite-free mother liquor was performed to remove excess reductant. These crystals remained colorless until treatment with DEA NONOate. During this treatment, the reduced, reductant-free, crystals were observed to change back to the yellowish light brown color of the as-isolated crystals, indicative of oxidation.

X-ray Diffraction Data Collection and Structure Determination. All X-ray diffraction data used for model building were acquired at 98 K at the Advanced Light Source, Berkeley, CA, on beamline 5.0.2 (X-ray wavelength, 0.97 Å). Two approaches were taken to obtain phases. First, a polyalanine model of the *D. gigas* ROO crystal structure (PDB ID 1E5D) was used for molecular replacement. Second, a redundant (760 deg of data) data set was collected at the University of Georgia on a Rigaku RU-200 rotating anode equipped with Osmic focusing mirrors and a R-axisIIc image plate detector using the oxidized crystals at 98 K (X-ray wavelength, 1.54 Å). Although these latter experiments provided diffraction data to only 3.5 Å nominal resolution, they were sufficient for single anomalous dispersion, from which eight potential iron positions were identified in the asymmetric unit. A reasonable solution for the phases was obtained by molecular replacement that was in good agreement with the iron positions. In all cases, no significant change in the color of the crystals was observed during the data collection, indicating that there was no change in the oxidation state of the crystal. Despite the poor diffraction, the crystals used in this study were fairly large (typically 0.2 mm × 0.2 mm × 0.5 mm).

During model building and refinement, the iron positions and the entire polypeptide were placed before the addition of the FMN cofactor or any water molecules. To avoid model bias, at no time during model building and refinement were constraints placed on the positions of the iron atoms. The oxidized (as-isolated) structure was refined first and the iron/peptide coordinates were used as a starting point for model building and refinement of the reduced and NO-treated FprA diffraction data sets. In the latter cases the peptide structure was modeled and refined prior to the addition of the FMN and water molecules. Subsequent rounds (15 for the as-isolated structure, 3 each for the dithionite-reduced and NO-reacted structures) of model building and refinement were performed using the programs O (*22*) and CNS (*23*). In all cases, the 4-fold noncrystallographic symmetry (NCS) observed in the asymmetric unit was used to improve the quality of the electron density maps. All statistics for data collection, model building, and refinement can be found in Table 1. Structure drawings were generated using the programs Molscript (*24*), Xtalview (*25*), Viewerlite (Accelrys, Inc.), Pymol (DeLano Scientific LLC), and Raster3D (*26*). Modeling of NO ligands was carried out using the builder module within the Spartan suite of programs (Wavefunction Inc., Irvine, CA).

Table 1: Data Collection and Refinement Statistics

	oxidized	reduced	NO-treated
Data Collection			
λ (Å)	1.0	1.0	1.0
resolution range (Å)	50.0−3.0	50.0−2.8	50.0−2.8
completeness (%)	99.9 (99.6)[b]	99.9 (99.3)	99.9 (96.0)
R_{sym}[a]	0.042 (0.17)	0.049 (0.26)	0.047 (0.19)
Refinement Statistics			
space group	$P4_32_12$	$P4_32_12$	$P4_32_12$
unit cell dimensions			
$a = b$ (Å)	159.6	159.6	160.3
c (Å)	276.7	278.1	279.1
refinement resolution (Å)	50.0−3.0	50.0−2.8	50.0−2.8
unique reflections	71781	88890	89051
R_{cryst} (%)	21.6	22.6	22.3
R_{free} (%)	25.9	24.5	24.5
protein atoms	12460	12460	12460
cofactor/nonprotein atoms	152	160	144
water atoms	61	132	282
residues in allowed region of Ramachandran plot (%)	99.0	98.2	98.8
rmsd from ideality			
bond distances	0.006	0.014	0.009
bond angles	1.42	1.91	1.62
B-factors (Å^2)			
average	55.9	52.9	64.6
minimum	12.3	30.8	37.2
maximum	132.8	200.0	152.0

[a] $R_{sym} = \sum_{hkl}[\sum_I(|I_{hkl,I} - \langle I_{hkl}\rangle|)]/\sum_{hkl,I}\langle I_{hkl}\rangle$, where I_{hkl} is the intensity of an individual measurement of the reflection with indices *hkl* and $\langle I_{hkl}\rangle$ is the mean intensity of that reflection. [b] The numbers in parentheses refer to the outer resolution bin used in data processing.

Site-Directed Mutagenesis. Plasmids encoding site-directed variants of *M. thermoacetica* FprA were constructed using the plasmid pFprA (*27*) as template and the QuikChange site-directed mutagenesis kit (Stratagene, Inc.) following the protocol described in the product manual and primers with the following nucleotide sequences: (listed 5′ to 3′ with the corresponding variant codon in italics): H86A, C GAA AGC GAT *GCT* GCC GGC GCC TTC CC; H25F, C CGC TAC TTC *TTC* GGT CCC GCT TTT TCC; Y195F, GAG GCG GCC AAG *TTC* TAT GCC AAT ATT CTC. Corresponding complementary primers were generated automatically by the manufacturer (Integrated DNA Technologies) using standard nucleotide pairing. The variant codons in the resulting plasmids, pH86A-FprA, pH25F-FprA, and pY195F-FprA, and pH25F,Y195F were verified by nucleotide sequencing at the University of Georgia Integrated Biotechnology Laboratories. The variant FprAs were expressed and purified following the protocol previously described for wild-type recombinant *M. thermoacetica* FprA (*9*). The purified variant proteins contained FMN and iron in amounts comparable to those of the wild-type protein.

RESULTS

Crystals of M. thermoacetica FprA. The crystal structures of three forms of *M. thermoacetica* FprA obtained using pH 6.5 precipitant are reported: oxidized (as-isolated, resolution 3.0 Å), anaerobic dithionite-reduced (reduced, resolution 2.8 Å), and anaerobic dithionite-reduced, nitric oxide-reoxidized (NO-reacted, resolution 2.8 Å). The crystal structure of as-isolated FprA obtained using a pH 4.5 precipitant (resolution 3 Å) was identical (including diiron ligands) to that obtained

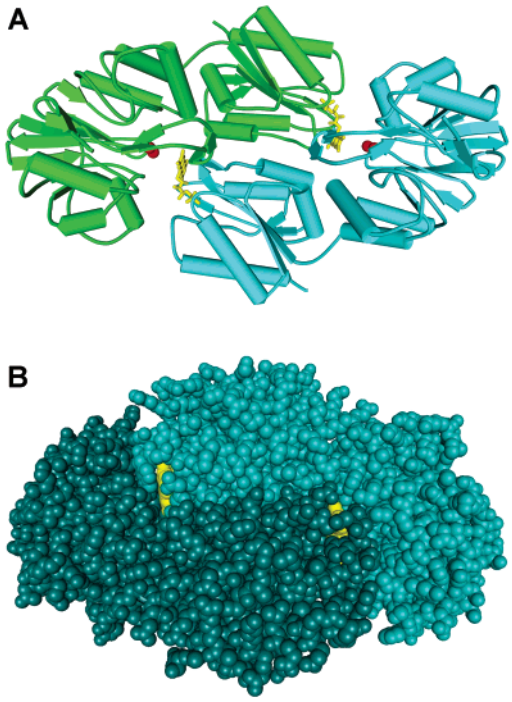

FIGURE 1: Panel A: Cartoon representation of the homodimer in crystalline *M. thermoacetica* FprA with one subunit colored green and the other cyan. Cylinders and arrowed ribbons represent helical and β-sheet backbone regions, respectively. Iron atoms are shown as red spheres, and FMN is shown in yellow ball-and-stick representation. Panel B: Space-filling representation of the *M. thermoacetica* FprA homodimer viewed along the pseudo-2-fold rotational axis with monomers colored different shades of blue. FMN atoms are shown in yellow.

using the pH 6.5 precipitant and is not further discussed. Typical crystals of as-isolated FprA and their UV−vis absorption spectrum are shown in Figure 1S (see Supporting Information). The spectrum of the as-isolated crystal is very similar to that recorded for the same FprA in solution prior to crystallization and is distinctly different from that of the Zn-substituted *M. thermoacetica* FprA (also shown in Figure 1S). For iron-containing FprA, the absorbance in the range 300−380 nm is higher than that at 450 nm ($A_{320}/A_{450} = 1.24$, comparable to 1.29 for the crystalline FprA spectrum in Figure 1S), whereas the opposite is true for the zinc-substituted FprA ($A_{320}/A_{450} = 0.45$) (*9*). The absorption spectrum of the as-isolated FprA crystal indicates that, although present at 100 mM in the mother liquor, zinc has not displaced iron in the active site and that the crystallization did not lead to reduction of the FprA. Anomalous scattering analysis (vide infra) confirmed diiron site occupancy by iron.

The *M. thermoacetica* FprA unit cell contains two homodimers, as opposed to the single homodimer found in the unit cell of the *D. gigas* ROO crystal structure (PDB file 1E5D). The association between the two *M. thermoacetica* homodimers, involving the metallo-β-lactamase-like domain of one homodimer and the flavodoxin domain of the other homodimer, appears to involve a very limited portion of the protein, is mediated by zinc (as determined by anomalous scattering) present in the crystallization buffer, and presumably has no physiological relevance. Neither NOR nor O_2R activities of as-isolated (i.e., iron-containing) FprA are Zn^{2+}-dependent, nor did added Zn^{2+} salts up to 200 mM inhibit these activities (data not shown). In solution, *M. thermoacetica* FprA is found to be a homodimer by gel filtration with no evidence for a tetramer (or any higher oligomers). No differences in the quaternary or tertiary structures were observed among the as-isolated, reduced, and NO-reacted forms of *M. thermoacetica* FprA crystals.

Tertiary and Quaternary Structures. The crystal structure of the *M. thermoacetica* FprA reveals a "head-to-tail" homodimer with two active sites consisting of the diiron site of one monomer in close contact with the FMN of the second monomer (Figure 1, panel A). The *M. thermoacetica* FprA tertiary and quaternary structures and the placement of cofactors are very similar to those reported for *D. gigas* ROO (*3*). A superposition of the *M. thermoacetica* FprA and *D. gigas* ROO homodimers gave an rms deviation of 1.87 Å for the α-carbon atoms of the two models. There are two, nonsymmetrical, copies of the dimer in the crystallographic asymmetric unit. The biological dimer is presented in Figure 1.

FMN Binding Site. As is the case for *D. gigas* ROO, the FMN cofactor in *M. thermoacetica* FprA is found at the interface between the two monomers of the homodimer. As shown in Figure 1, panel B, the O═C−NH−C═O portion of the FMN isoalloxazinic ring is visible from the outer surface of the protein in a space-filling representation of the *M. thermoacetica* FprA homodimer. Steric crowding by the protein on both sides of the isoalloxazinic ring plane effectively precludes direct interaction with NADH, which typically involves aromatic ring stacking between the nicotinamide and the FMN. This structural feature explains why NADH does not directly reduce the FprA FMN (*9*). Most of the protein atoms in close contact (within 4.5 Å) with the FMN belong to one monomer. Atoms from four residues of the second monomer within the homodimer are also in close contact with the FMN. These latter residues are at or near the diiron site: E83, H148 (diiron ligands), H25 (substrate binding pocket; see below), and W149 (in close contact with H148). The shortest interatomic distance between the FMN and diiron site atoms is <4 Å and occurs between the non-iron-bound oxygen of the E83 carboxylate ligand and an FMN methyl group.

Diiron Site. As is the case for *D. gigas* ROO, the diiron site and its ligands are completely buried in the protein interior. Figure 2 shows the diiron site and the anomalous scattering for data collected at 1.54 Å on as-isolated FprA crystals. The presence of a significant anomalous scattering signal at this wavelength, together with the absence of a 1.54 Å anomalous scattering signal from the putative Zn^{2+}-occupied site between homodimers, is consistent with the two metals in Figure 2 being iron. The Zn^{2+}-occupied sites in all of the models have been further confirmed by the appearance of strong anomalous signals when data were collected at 0.98 Å.

Figure 3 shows a superposition of the *D. gigas* ROO and as-isolated *M. thermoacetica* FprA active sites, together with a schematic depiction of the diiron coordination sphere in the latter protein. Table 2 compares the iron−ligand and iron−iron interatomic distances in the two proteins. The electron density maps for all three *M. thermoacetica* FprA crystal structures (as-isolated, reduced, NO-reacted) are consistent with the presence of a solvent bridge between the two iron atoms. The resolution of these structures are too low to provide evidence for protonation states of this bridge

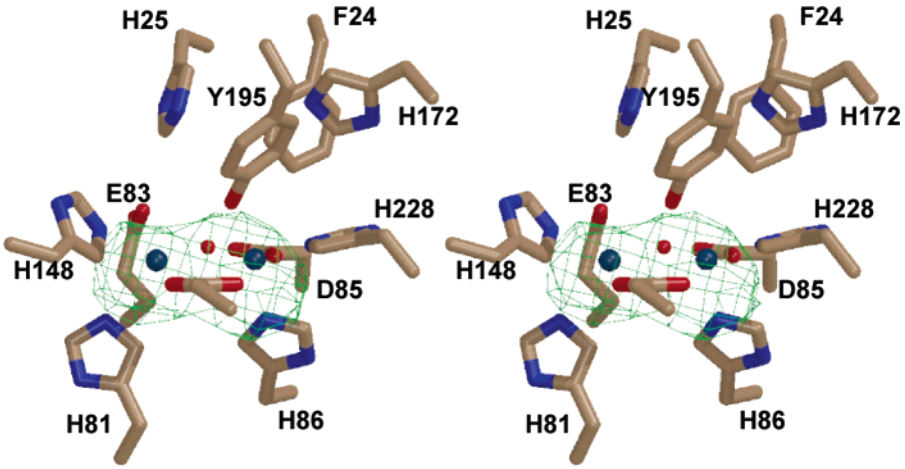

FIGURE 2: Anomalous scattering signal contoured at 8σ for data collected at 1.54 Å superimposed over a wall-eyed stereoview of model for the active site of as-isolated *M. thermoacetica* FprA. Iron atoms and hydroxo are shown as spheres; other atoms are shown in ball-and-stick representation. Carbon, oxygen, nitrogen, and iron atoms are colored tan, red, blue, and green, respectively.

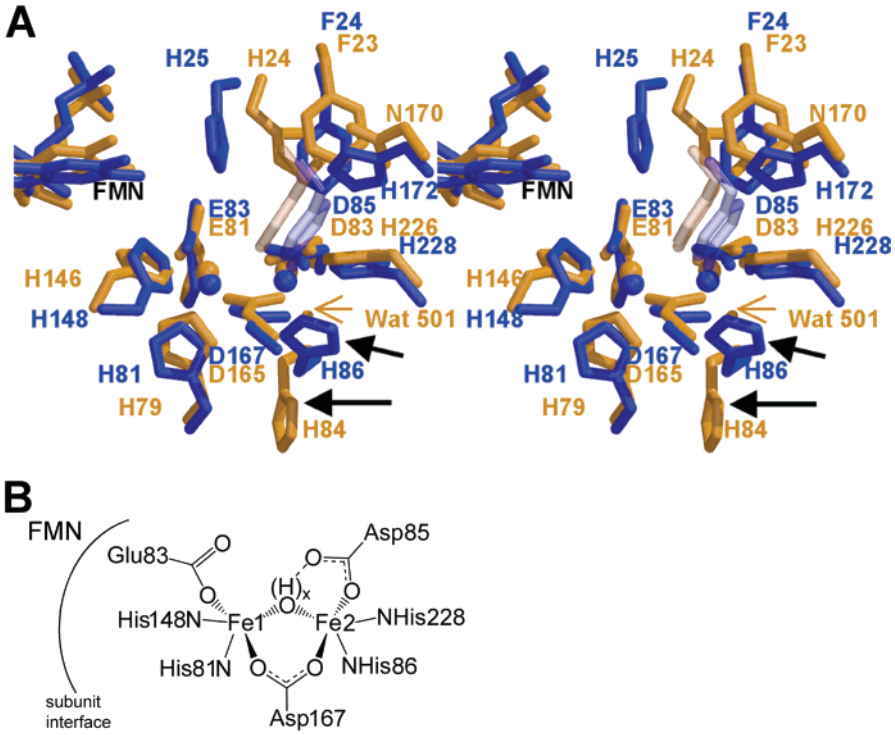

FIGURE 3: Panel A: Wall-eyed stereoview of the *D. gigas* ROO (orange; PDB ID 1E5D) and *M. thermoacetica* FprA (blue) diiron sites and surrounding residues from a best fit superposition of the two protein backbones (rms deviation 1.87 Å). Iron atoms and water (orange arrow) are shown as spheres, while the other atoms are shown in ball-and-stick representation. The differing positions of H84 and H86 side chains are highlighted by the black arrows. The side chain of a structurally conserved tyrosine (Y195 in FprA and Y193 in ROO, unlabeled and approximately in the middle of the figure) has been made transparent for clarity. Panel B: Schematic depiction of the diiron coordination sphere in *M. thermoacetica* FprA.

(i.e., oxo, hydroxo, or aquo). A hydroxo bridge was previously inferred for the as-isolated *M. thermoacetica* FprA in solution, based on UV−vis absorption and Mössbauer spectroscopies (*9*). A solvent bridge between the irons was also included in the crystal structure of *D. gigas* ROO (*3*).

The amino acid residues furnishing diiron ligands are homologous and appear to occupy positions similar to those in *D. gigas* ROO *with the notable exception of H86*. The analogous residue, H84, in *D. gigas* ROO appears to have swung away from the iron and is replaced by a solvent ligand (WAT501 in Figure 3). Figure 4 shows a composite omit map focusing on electron density around H86, which confirms that its side chain is within ligating distance of Fe2 in *M. thermoacetica* FprA. The ligation of H86 does not appear to be redox-dependent, since H86 remains a ligand in the as-isolated, reduced, and NO-reacted *M. thermoacetica* FprA crystals. An H86A variant of *M. thermoacetica* FprA was expressed in *E. coli* only as inclusion bodies. The apparent deligation of the H86 homologue in *D. gigas* ROO is unlikely to be pH-dependent, since the ROO crystals were reportedly obtained at pH ~6 (*3*), which is within the range of the pH 4.5−6.5 precipitants used to obtain the *M. thermoacetica* FprA crystals. The deligated H86 homologue in *D. gigas* ROO (H84) does not appear to be stabilized by any interaction (H-bonding, etc.) from its immediate environment. Thus, our data do not readily suggest structural, acid−

Table 2: Iron−Ligand and Iron−Iron Interatomic Distances (Å) for *M. thermoacetica* FprA (This Work) and *D. gigas* ROO (*3*)

		M. thermoacetica FprA		
distances[a]	*D. gigas* ROO	as isolated	reduced	NO-reacted
Fe1−Fe2	3.36, 3.37	3.30, 3.31, 3.31, 3.34	3.28, 3.35, 3.23, 3.46	3.23, 3.33, 3.33, 3.57
Fe1−E83 OE1	2.04, 2.04	2.25, 2.74, 1.94, 1.91	2.31, 2.30, 2.29, 2.01	2.33, 2.19, 2.08, 1.83
Fe1−H148 NE2	2.08, 2.08	2.24, 2.06, 2.34, 2.23	2.33, 2.35, 2.47, 2.34	2.42, 2.40, 2.49, 2.29
Fe1−H81 NE2	2.14, 2.13	2.67, 2.43, 2.44, 2.37	2.44, 2.39, 2.33, 2.37	2.36, 2.33, 2.19, 2.38
Fe1−D167 OD2	1.93, 1.93	2.04, 2.16, 2.03, 2.05	2.17, 2.29, 2.12, 2.08	2.16, 2.30, 2.10, 2.17
Fe1−O_{solv}[b]	2.25, 2.26	2.04, 2.04, 2.04, 2.05	2.03, 2.03, 2.02, 2.06	1.98, 2.00, 2.00, 2.03
Fe2−D85 OD2	2.32, 2.33	2.19, 2.11, 2.12, 2.23	2.32, 2.16, 2.32, 2.22	2.27, 2.04, 2.09, 2.08
Fe2−H228 NE2	2.02, 2.02	1.98, 2.11, 2.01, 2.05	2.13, 2.16, 2.11, 2.15	2.24, 2.17, 1.99, 2.11
Fe2−H86 NE2[c]	5.99, 5.96	2.09, 2.06, 2.28, 2.21	2.25, 2.18, 2.35, 2.22	2.14, 2.17, 2.36, 2.21
	2.43, 2.59			
Fe2−D167 OD1	2.05, 2.06	2.09, 1.95, 2.05, 2.17	2.26, 2.37, 2.32, 2.31	2.30, 2.30, 2.24, 2.36
Fe2−WAT501[c]	1.75, 1.76	2.03, 2.03, 2.03, 2.04	2.05, 2.03, 2.02, 2.05	2.00, 2.00, 1.95, 2.04
Fe1−X[d]	2.73, 3.11	2.99, 3.31, 3.06, 2.91	3.19, 3.24, 3.02, 3.18	3.54, 3.45, 3.21, 3.25
Fe2−X[d]	2.60, 2.61	2.92, 2.57, 3.17, 2.37	2.66, 2.78, 3.56, 3.41	3.21, 3.06, 3.24, 3.09

[a] Residue numbering as in *M. thermoacetica* FprA. Distances are listed for each monomer in the asymmetric unit in the order A, B, C, D. [b] Distance to the bridging solvent molecule. [c] Shown in italics is the distance between Fe2 and its WAT501 solvent ligand in *D. gigas* ROO. [d] Distance to the closest atom of the exogenous ligand, "X", ethylene glycol, or water (see text).

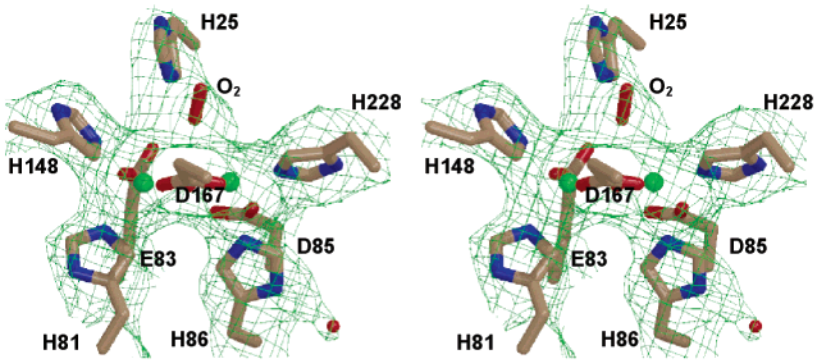

FIGURE 4: Wall-eyed stereoview of the $2F_o - F_c$ composite omit map contoured at 1.0σ superimposed on the ball-and-stick model for the diiron site in as-isolated *M. thermoacetica* FprA crystals. The composite omit map was generated using the simulated annealing protocol with 5% of the model being omitted at a time. Atoms are color-coded as listed in the legend to Figure 2.

base, or redox explanations for the differing H86/H84 ligation in the two proteins. In any case, both iron atoms in the diiron site of *M. thermoacetica* FprA are five-coordinate with the unoccupied sixth coordination positions approximately trans to H81 and H86. These empty coordination positions are an obvious choice for NO binding. In the *D. gigas* ROO crystal structure, the analogous coordination positions of the two irons trans to H81 and WAT501 were also empty and inferred to be involved in O_2 binding (*3*).

Based partly on the precedent of the *D. gigas* ROO structure, we modeled the additional density above the diiron site in Figure 4 for the as-isolated (all-ferric) *M. thermoacetica* FprA as a dioxygen molecule. No constraints on the iron atoms or the dioxygen molecule were used during refinement. When the model was refined with a water rather than dioxygen molecule in this position, the *R* values increased by 0.8%, and a 4σ peak appeared in the $1F_o - F_c$ omit map. The density is too small to accommodate ethylene glycol or acetate, the only known buffer components that are potential candidates for this density. The resolution of the data, however, prevents an accurate description of potential interactions of the putative diatomic molecule with pocket residues and does not rule out the possibility that this density is due to an unknown buffer component.

As shown in Table 2, the average Fe1−Fe2 distance in the as-isolated *M. thermoacetica* FprA crystals is 3.2 Å, which is slightly shorter than the corresponding 3.4 Å previously reported in the crystal structure of *D. gigas* ROO. To ascertain that the Fe1−Fe2 distance in *M. thermoacetica* FprA did not significantly lengthen upon reduction, fits to the data for the reduced FprA were attempted with models having significantly longer or shorter Fe1−Fe2 distances. In this case the Fe1−Fe2 distance of the reduced model was constrained at either longer or shorter separations and a $1F_o - F_c$ composite omit map was generated (cf. Figure 2S). When an Fe1−Fe2 distance of 2.9 Å was assumed in the model, a strong peak developed between the two irons in the $1F_o - F_c$ composite omit map, suggesting that such a model places too much electron density in this area. Conversely, when a fixed Fe1−Fe2 distance of 3.8 Å was used in the model, similar peaks developed outside the diiron site in the $1F_o - F_c$ difference map, suggesting that such a structure places too much electron density along the Fe1−Fe2 axis on the outer edges of the diiron site. These fits are thus consistent with the average 3.3 Å Fe1−Fe2 distance for reduced (presumably diferrous) *M. thermoacetica* FprA listed in Table 2. Similarly, the NO-reacted (presumably diferric) FprA shows an average Fe1−Fe2 distance of 3.4 Å.

Similarly to the as-isolated FprA difference map shown in Figure 4, the electron density map from reduced *M. thermoacetica* FprA crystals (cf. Figure 5, panel A) also

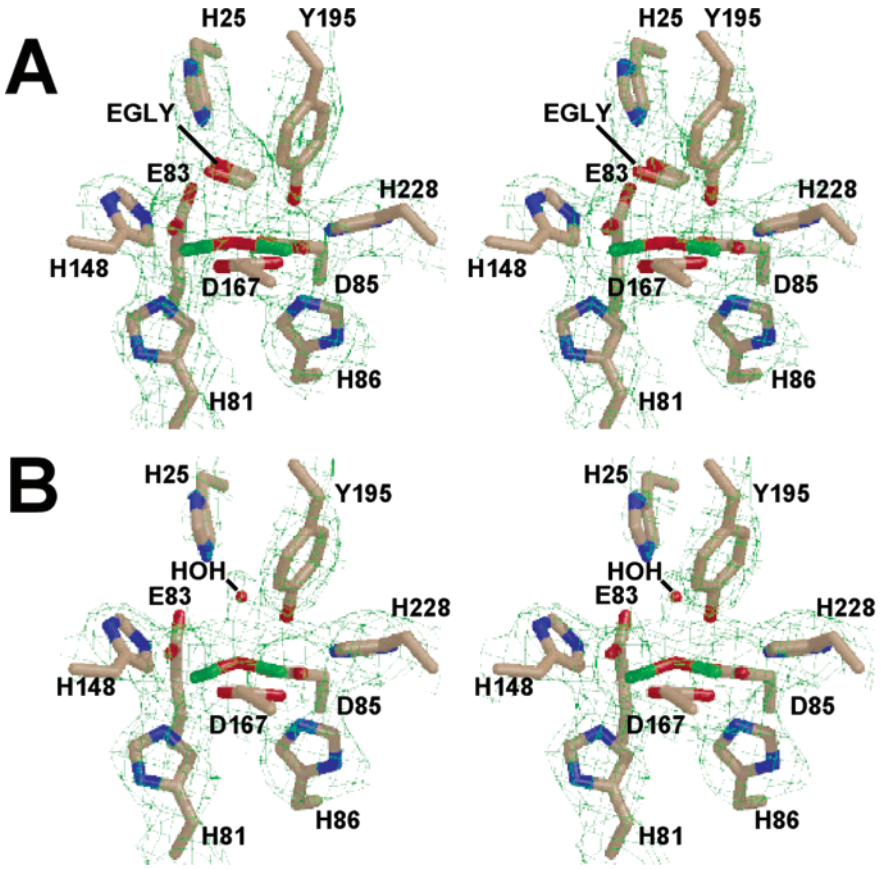

FIGURE 5: Wall-eyed stereoviews of $2F_o - F_c$ composite omit maps contoured at 1.0σ for the reduced (panel A) and reduced, NO reacted (panel B) *M. thermoacetica* FprA diiron sites. In both cases the maps were generated using the simulated annealing protocol with 5% of the model being omitted per cycle. The electron density is superimposed on the ball-and-stick models of the diiron site including either an ethylene glycol (EGLY in panel A) or a water (HOH in panel B) molecule in the cavity above the Fe−O(H)$_x$−Fe plane. Color coding of atoms is as listed in the legend to Figure 2.

showed "extra" density above the diiron site. In this case, however, the electron density is larger and could be better fit as an ethylene glycol molecule rather than a diatomic molecule. This modeling is consistent with the use of ethylene glycol as cryoprotectant when freezing the crystals and implies that reduction allows greater access to the active site. The closest atoms of the modeled ethylene glycol are too far away to furnish ligands to Fe1 or Fe2 (cf. Table 2) but could be within hydrogen-bonding distance of His25 NE2. The cis conformation of the modeled ethylene glycol is not unusual in protein crystals (*28*, *29*). The best fit to the electron density has the C−C bond axis of the ethylene glycol approximately perpendicular to the Fe1−Fe2 axis. As shown in Figure 5, panel B, the electron density modeled as ethylene glycol in the reduced FprA structure disappeared almost completely in the NO-reacted structure. The residual electron density above the diiron site in the NO-reacted crystals is more consistent with a solvent molecule hydrogen-bonded to the bridging solvent ligand. This change in electron density above the diiron site is consistent with displacement of ethylene glycol by NO, followed by reduction of NO at the diiron site with the product of this reduction (N_2O) leaving the site before the crystal was frozen. The diiron site in Figure 5, panel B, should thus be in the diferric state. This conclusion is supported by the rapid reduction rate of NO by FprA (*9*), the observation of a color change indicating oxidation of the dithionite-reduced, NO-treated crystals, and the time it took to freeze the crystals (several minutes) following NO treatment.

Figure 6, panel A, shows a space-filling model of the pocket above the FprA diiron site that was modeled as occupied by O_2, ethylene glycol, or solvent in the *M. thermoacetica* FprA structures. These occupancies are, of course, sterically consistent with occupancy of this pocket by NO and/or N_2O. Open sixth coordination positions on Fe1 and Fe2 are oriented toward each other and toward the pocket above the FprA diiron site [i.e., above the Fe−O(H)$_x$−Fe plane]. Figure 6, panel B, illustrates how this pocket can accommodate a diferrous dinitrosyl in which the NO molecules are N-coordinated terminally to the sixth coordination positions on Fe1 and Fe2 with Fe−N−O angles of 167°, Fe−NO distances of 1.75 Å, N−O distances of 1.16 Å, and a N- - -N distance between the coordinated NOs of 2.80 Å. These distances and angles mimic those of a previously described synthetic, carboxylate-bridged diferrous dinitrosyl complex (*30*). Side chains of H25, Y195, H172, and F24 all have atoms within ~3 Å from either atom of the two modeled NOs. Rotation of the coordinated NO molecules around the Fe−NO axes at a fixed Fe−N−O angle of 167° appears to be sterically permitted, as do more acute Fe−N−O angles [down to at least 144°, as observed in some synthetic non-heme ferrous nitrosyl complexes (*31*, *32*)]. A diferrous mononitrosyl, where one NO is coordinated as described above and a second noncoordinating NO sits above the diiron site, was also successfully modeled with no steric conflicts. Several narrow channels may provide pathways for diffusion of NO and N_2O between the diiron site pocket and the protein surface (*33*).

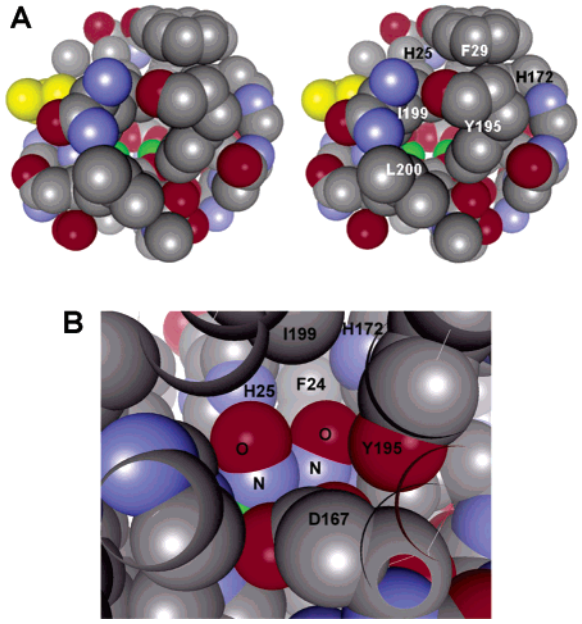

FIGURE 6: The substrate binding pocket and proposed NO binding model. Panel A: Wall-eyed stereoview of space-filling representation of the cavity above the diiron site occupied by ethylene glycol in the reduced *M. thermoacetica* FprA structure (with ethylene glycol omitted for clarity). Panel B: Diferrous dinitrosyl modeled into the reduced *M. thermoacetica* FprA structure. Atoms are color-coded as follows: iron, green; oxygen, red; nitrogen, blue; carbon, gray; FMN, yellow.

Evidence for Involvement of Pocket His and Tyr in NOR Catalysis. As shown in Figures 2−6, several residues line a pocket above the two unoccupied iron coordination positions. The identity and position of the pocket residue Y195 in *M. thermoacetica* FprA are conserved as Y193 in *D. gigas* ROO (cf. Figure 3). The pocket residue H25 in *M. thermoacetica* FprA (H24 in *D. gigas* ROO) is also conserved, but its side chain appears slightly displaced in the superposition of the two structures (possibly due to the presence of an "extra" Y26 in *D. gigas* ROO; cf. Figure 3). The H25 Nϵ and Y195 phenolic OH atoms are within hydrogen-bonding distance of the modeled NOs in Figure 6, panel B. Consistent with involvement of these residues in NOR catalysis, Figure 3S shows that the H25F and Y195F variants of *M. thermoacetica* FprA exhibit decreased NOR activities and that this decrease is due to a lower k_{cat} and not to a significantly higher K_M relative to wild-type FprA. Both variants had a K_M of ~7 μM compared to 4 μM for the wild-type protein, whereas k_{cat} was 7 s^{-1} for Y195F and 1.4 s^{-1} for H25F, compared to 48 s^{-1} for wild type (*9*). Similarly lowered activity relative to wild type was observed for the double H25F,Y195F FprA variant.

DISCUSSION

The crystal structures of *M. thermoacetica* FprA show a diiron site with two "two-His" iron centers rather than the two-His and "one-His" iron centers found in the *D. gigas* ROO crystal structure. As shown in Figure 3, the side chain of the fourth His ligand residue, H86, in *M. thermoacetica* FprA is conserved as H84 in *D. gigas* ROO but is rotated away from the diiron site. An amino acid sequence alignment reveals that the residue corresponding to H86/84 is conserved in all but four of the ~100 FprA homologues in the NCBI database (*33*),[2] which together with the ligation of H86 to iron found in this work indicates a crucial role for this residue. The H86 ligand is retained in the as-isolated, reduced, and NO-reacted *M. thermoacetica* FprA and is also retained in crystals prepared using either pH 4.5 or pH 6.5 precipitants. Only the as-isolated, presumably diferric, structure of *D. gigas* ROO has been reported (using a pH ~6 precipitant) (*3*), and O_2R is the only activity that has been reported for the *D. gigas* ROO. Other FprAs are irreversibly inactivated during O_2R turnover (*7*, *9*, *10*). The apparent loss of the H84 diiron ligand in the *D. gigas* ROO crystal structure could conceivably occur during ROO's irreversible inactivation resulting from adventitious O_2R turnover during aerobic isolation and purification from the *D. gigas* cell extract. That is, the "H84-off" diiron site may represent an FprA that is inactive both as an O_2R and as a NOR. The reactivity of *D. gigas* ROO with NO has not been reported, and our results do not rule out the possibility that the H84-off diiron site correlates with an O_2R function in vivo. However, we have shown that an FprA with 57% amino acid sequence identity to *D. gigas* ROO (including the diiron ligand residues and H84 homologue) from the taxonomically closely related *D. vulgaris* protects an NO-hypersensitive *E. coli* strain from NO-induced death under anaerobic growth conditions (*10*). The recombinant *D. vulgaris* FprA also shows in vitro NOR activity and self-inactivating O_2R activity, similarly to those of other characterized FprAs. We, therefore, anticipate an NOR function for *D. gigas* ROO using the "H84-on" diiron site. Some parallels between the FprA/dioxygen-activating non-heme diiron enzymes are found in the bacterial respiratory NORs/cytochrome *c* oxidases. The bacterial respiratory NORs structurally resemble cytochrome *c* oxidases, but with a heme, non-heme diiron rather than heme, copper active site (*12*, *13*). These respiratory NORs also show O_2R activity, but with much lower catalytic efficiencies than for NOR activity (*13*).

It is clear that diatomic molecules can occupy a pocket directly above the open coordination positions at the diiron sites in both *D. gigas* ROO and *M. thermoacetica* FprA and that a larger molecule, such as ethylene glycol, can also occupy this pocket in at least the latter protein (cf. Figure 5). The modeled structure in Figure 6, panel B, shows that a diferrous dinitrosyl, which is a proposed catalytic intermediate (cf. Scheme 2), is also sterically feasible. The modeled, coordinated NOs are in close contact with several side chains lining the pocket, including that of H25. The ~30-fold lower k_{cat} for NOR activity of an H25F *M. thermoacetica* FprA variant indicates a role for this diiron pocket residue in the breakdown of the catalytically competent intermediate, the most likely being protonation of the diferrous dinitrosyl. H25 is conserved in approximately half of the ~100 FprA amino acid sequences, including *D. gigas* ROO (cf. Figure 3), with the vast majority of the remainder containing a glutamate or aspartate at this position (*33*). A

[2] The deduced amino acid sequences of four cyanobacterial FprA homologues contain an arginine at the residue aligning with H86 in *M. thermoacetica* FprA. This substitution is invariably accompanied by substitution of an N,N or S,N pair for E83,D85, which also furnish diiron ligands in *M. thermoacetica* FprA. These multiple diiron ligand substitutions indicate a significantly different active site structure for these cyanobacterial homologues.

Scheme 3

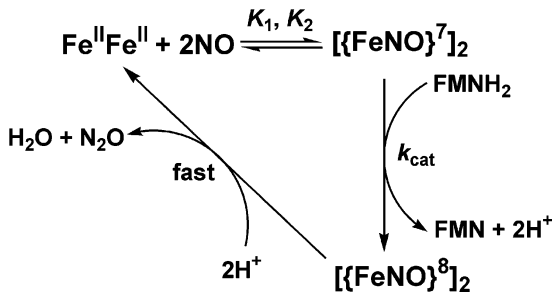

lysine is present at this position in two *Methanococcus jannaschi* FprA homologues . Thus, a potentially proton-donating residue is conserved at this position in all known FprAs (the lone exception being the FprA from *Treponema denticola*, which contains phenylalanine at this position). A similar analysis applies to the diiron pocket residue Y195 of *M. thermoacetica* FprA, the F195 variant of which also showed a lowered NOR k_{cat}. Y195 is conserved in all but three of the ~100 FprA amino acid sequences (*33*).

The conserved Fe1 and Fe2 coordination spheres and fixed Fe1- - -Fe2 distance of 3.3 ± 0.1 Å upon redox interconversion and reaction with nitric oxide in *M. thermoacetica* FprA are consistent with efficient formation of nitrous oxide via a diferrous dinitrosyl. By contrast, reduction of diferric sites to diferrous in other non-heme diiron proteins with histidine and carboxylate ligands, such as rubrerythrin and ribonucleotide reductase, results in lengthening of the Fe−Fe distance by up to ~0.7 Å, to ~4 Å in the diferrous state accompanied by changes in coordination number and/or geometry (*34*, *35*). Perhaps symptomatically, these other diiron proteins catalyze *O−O bond-breaking* reactions, rather than the *bond-forming* NOR reaction. Although *E. coli* ribonucleotide reductase forms a diferrous dinitrosyl, this adduct only slowly and noncatalytically decomposes to release N_2O (*36*). Nitric oxide adducts of rubrerythrin have not been reported. The diferrous site of another O_2-activating enzyme, methane monooxygenase, reacts with nitric oxide similarly to ribonucleotide reductase, i.e., forming a diferrous dinitrosyl followed by slow, noncatalytic release of N_2O (*37*). Although the Fe1−Fe2 distance in methane monooxygenase apparently does not vary by more than ~0.2 Å between the resting diferric and diferrous states, the coordination geometry and ligation of both irons do change significantly upon diferrous/diferric interconversion (*38*). Thus, the retention of its diiron coordination environment and Fe1- - -Fe2 distance upon redox interconversion, its catalytic NOR activity, and its aerobic inactivation all support a NOR function for *M. thermoacetica* FprA.

The fact that the H25F,Y195F variant retained significant NOR activity suggests that events in addition to protonation of an intermediate may be required for catalytic NOR turnover. We propose that "super-reduction" of the diferrous dinitrosyl by $FMNH_2$ occurs during the k_{cat} step, as diagramed in Scheme 3, in which the diferrous dinitrosyl $[\{FeNO\}^7]_2$ in the Enemark−Feltham notation (*39*)] is reduced to $[\{FeNO\}^8]_2$. The $\{FeNO\}^8$ species would be significantly more basic and, therefore, much more readily protonated (*40*). In fact, the transient $[\{FeNO\}^8]_2$ species in Scheme 3 could alternatively be formulated as the diprotonated form, $[\{FeNO(H)\}^8]_2$, consistent with the release of two protons upon oxidation of $FMNH_2$. Scheme 3 also rationalizes why an active site capable of storing four accessible reducing equivalents (two in FMN plus two in the diiron site) is needed to catalyze the two-electron reduction of 2NO to N_2O. In the reduced, NO-reacted FprA crystal, a "single turnover" would reduce 2NO to N_2O, yielding a two-electron reduced active site that could then react with two more equivalents of NO to give initially an $[[\{FeNO\}^7]_2$, oxidized FMN] active site, the diferrous dinitrosyl then more slowly converting to diferric plus N_2O.

A mechanism analogous to Scheme 3 can be written for O_2R turnover by substituting one dioxygen for two nitric oxide molecules. In this case inactivation could result from reaction of a two-electron reduced active site with dioxygen to give a highly oxidizing diferric peroxo and/or diferryl ($[(Fe^{IV}{=}O)^{2+}]_2$) species, as occurs in the dioxygen-activating non-heme diiron enzymes (*41*). The results reported herein provide new insight into the structural features that nature has adopted to fine-tune biological non-heme diiron sites for dioxygen activation vs nitric oxide reduction.

ACKNOWLEDGMENT

R.S.-D. thanks the Chemistry Department of Babeş-Bolyai University, Cluj-Napoca, Romania, for a leave of absence.

SUPPORTING INFORMATION AVAILABLE

Figures showing UV−vis absorption spectrum of *M. thermoacetica* FprA crystal, difference maps used to position the iron atoms in the reduced FprA model, and Michaelis−Menten plots of NOR activities for H25F and Y195F variants. This material is available free of charge via the Internet at http://pubs.acs.org.

REFERENCES

1. Wasserfallen, A., Ragettli, S., Jouanneau, Y., and Leisinger, T. (1998) A family of flavoproteins in the domains Archaea and Bacteria, *Eur. J. Biochem. 254*, 325−332.
2. Gomes, C. M., Frazao, C., Xavier, A. V., Legall, J., and Teixeira, M. (2002) Functional control of the binuclear metal site in the metallo-beta-lactamase-like fold by subtle amino acid replacements, *Protein Sci. 11*, 707−712.
3. Frazão, C., Silva, G., Gomes, C. M., Matias, P., Coelho, R., Sieker, L., Macedo, S., Liu, M. Y., Oliveira, S., Teixeira, M., Xavier, A. V., Rodrigues-Pousada, C., Carrondo, M. A., and Le Gall, J. (2000) Structure of a dioxygen reduction enzyme from *Desulfovibrio gigas*, *Nat. Struct. Biol. 7*, 1041−1045.
4. Gomes, C. M., Vicente, J. B., Wasserfallen, A., and Teixeira, M. (2000) Spectroscopic studies and characterization of a novel electron-transfer chain from *Escherichia coli* involving a flavorubredoxin and its flavoprotein reductase partner, *Biochemistry 39*, 16230−16237.
5. Chen, L., Liu, M. Y., LeGall, J., Fareleira, P., Santos, H., and Xavier, A. V. (1993) Rubredoxin oxidase, a new flavo-hemoprotein, is the site of oxygen reduction to water by the "strict anaerobe" *Desulfovibrio gigas*, *Biochem. Biophys. Res. Commun. 193*, 100−105.
6. Chen, L., Liu, M. Y., Legall, J., Fareleira, P., Santos, H., and Xavier, A. V. (1993) Purification and characterization of an NADH-rubredoxin oxidoreductase involved in the utilization of oxygen by *Desulfovibrio gigas*, *Eur. J. Biochem. 216*, 443−448.
7. Gardner, A. M., Helmick, R. A., and Gardner, P. R. (2002) Flavorubredoxin, an inducible catalyst for nitric oxide reduction and detoxification in *Escherichia coli*, *J. Biol. Chem. 277*, 8172−8177.
8. Mukhopadhyay, P., Zheng, M., Bedzyk, L. A., LaRossa, R. A., and Storz, G. (2004) Prominent roles of the NorR and Fur

regulators in the *Escherichia coli* transcriptional response to reactive nitrogen species, *Proc. Natl. Acad. Sci. U.S.A. 101*, 745−750.
9. Silaghi-Dumitrescu, R., Coulter, E. D., Das, A., Ljungdahl, L. G., Jameson, G. N., Huynh, B. H., and Kurtz, D. M., Jr. (2003) A flavodiiron protein and high molecular weight rubredoxin from *Moorella thermoacetica* with nitric oxide reductase activity, *Biochemistry 42*, 2806−2815.
10. Silaghi-Dumitrescu, R., Ng, K. Y., Viswanathan, R., and Kurtz, D. M., Jr. (2005) A flavodiiron protein from *Desulfovibrio vulgaris* with oxidase and nitric oxide reductase activities. Evidence for an in vivo nitric oxide scavenging function, *Biochemistry 44*, 3572−3579.
11. Büsch, A., Pohlmann, A., Friedrich, B., and Cramm, R. (2004) A DNA region recognized by the nitric oxide-responsive transcriptional activator NorR is conserved β-and γ-proteobacteria, *J. Bacteriol. 186*, 7980−7987.
12. Hendriks, J., Oubrie, A., Castresana, J., Urbani, A., Gemeinhardt, S., and Saraste, M. (2000) Nitric oxide reductases in bacteria, *Biochim. Biophys. Acta 1459*, 266−273.
13. Wasser, I. M., de Vries, S., Moënne-Loccoz, P., Schrèoder, I., and Karlin, K. D. (2002) Nitric oxide in biological denitrification: Fe/Cu metalloenzyme and metal complex NO_x redox chemistry, *Chem. Rev. 102*, 1201−1234.
14. Poock, S. R., Leach, E. R., Moir, J. W., Cole, J. A., and Richardson, D. J. (2002) Respiratory detoxification of nitric oxide by the cytochrome *c* nitrite reductase of *Escherichia coli*, *J. Biol. Chem. 277*, 23664−23669.
15. Corker, H., and Poole, R. K. (2003) Nitric oxide formation by *Escherichia coli*. Dependence on nitrite reductase, the NO-sensing regulator Fnr, and flavohemoglobin Hmp, *J. Biol. Chem. 278*, 31584−92.
16. Haveman, S. A., Greene, E. A., Stilwell, C. P., Voordouw, J. K., and Voordouw, G. (2004) Physiological and gene expression analysis of inhibition of *Desulfovibrio vulgaris* Hildenborough by nitrite, *J. Bacteriol. 186*, 7944−7950.
17. Vicente, J. B., Gomes, C. M., Wasserfallen, A., and Teixeira, M. (2002) Module fusion in an A-type flavoprotein from the cyanobacterium *Synechocystis* condenses a multiple-component pathway in a single polypeptide chain, *Biochem. Biophys. Res. Commun. 294*, 82−87.
18. Seedorf, H., Dreisbach, A., Hedderich, R., Shima, S., and Thauer, R. K. (2004) $F_{420}H_2$ oxidase (FprA) from *Methanobrevibacter arboriphilus*, a coenzyme F_{420}-dependent enzyme involved in O_2 detoxification, *Arch. Microbiol. 182*, 126−137.
19. Gomes, C. M., Giuffre, A., Forte, E., Vicente, J. B., Saraiva, L. M., Brunori, M., and Teixeira, M. (2002) A novel type of nitric oxide reductase. *Escherichia coli* flavorubredoxin, *J. Biol. Chem. 277*, 25273−25276.
20. Drake, H. L., and Daniel, S. L. (2004) Physiology of the thermophilic acetogen *Moorella thermoacetica*, *Res. Microbiol. 155*, 422−436.
21. Seifritz, C., Daniel, S. L., Gossner, A., and Drake, H. L. (1993) Nitrate as a preferred electron sink for the acetogen *Clostridium thermoaceticum*, *J. Bacteriol. 175*, 8008−8013.
22. Jones, T., Zou, J., Cowan, S., and Kjeldgaard, M. (1991) Improved methods for building protein models in electron density maps and the location of errors in these models, *Acta Crystallogr. A 47*, 110−119.
23. Brünger, A. T., Adams, P. D., Clore, G. M., DeLano, W. L., Gros, P., Grosse-Kunstleve, R. W., Jiang, J. S., Kuszewski, J., Nilges, M., Pannu, N. S., Read, R. J., Rice, L. M., Simonson, T., and Warren, G. L. (1998) Crystallography & NMR system: A new software suite for macromolecular structure determination, *Acta Crystallogr., Sect. D: Biol. Crystallogr. 54*, 905−921.
24. Kraulis, P. J. (1991) Molscript−a program to produce both detailed and schematic plots of protein structures, *J. Appl. Crystallogr. 24*, 946−950.
25. McRee, D. E. (1999) XtalView/Xfit−A versatile program for manipulating atomic coordinates and electron density, *J. Struct. Biol. 125*, 156−165.
26. Merritt, E. A., and Murphy, M. E. P. (1994) Raster3d version 2.0−a program for photorealistic molecular graphics, *Acta Crystallogr. D 50*, 869−873.
27. Das, A., Coulter, E. D., Kurtz, D. M., Jr., and Ljungdahl, L. G. (2001) Five-gene cluster in *Clostridium thermoaceticum* consisting of two divergent operons encoding rubredoxin oxidoreductase-rubredoxin and rubrerythrin-type A flavoprotein-high-molecular-weight rubredoxin, *J. Bacteriol. 183*, 1560−1567.
28. Laskowski, R. A., Hutchinson, E. G., Michie, A. D., Wallace, A. C., Jones, M. L., and Thornton, J. M. (1997) PDBsum: a Web-based database of summaries and analyses of all PDB structures, *Trends Biochem. Sci. 22*, 488−490.
29. Kadziola, A., Abe, J., Svensson, B., and Haser, R. (1994) Crystal and molecular structure of barley alpha-amylase, *J. Mol. Biol. 239*, 104−121.
30. Feig, A. L., Bautista, M. T., and Lippard, S. J. (1996) A carboxylate-bridged non-heme diiron dinitrosyl complex, *Inorg. Chem. 35*, 6892−6898.
31. Brown, C. A., Pavlosky, M. A., Westre, T. E., Zhang, Y., Hedman, B., Hodgson, K. O., and Solomon, E. I. (1995) Spectroscopic and theoretical description of the electronic structure of $S = {}^3/_2$ iron-nitrosyl complexes and their relation to O_2 activation by non-heme iron enzyme active sites, *J. Am. Chem. Soc. 117*, 715−732.
32. Li, M., Bonnet, D., Bill, E., Neese, F., Weyhermuller, T., Blum, N., Sellman, D., and Wieghardt, K. (2002) Tuning the electronic structure of octahedral iron complexes [FeL(X)] (L = 1-alkyl-4,7-bis(4-*tert*-butyl-2-mercaptobenzyl)-1,4,7-triazacyclononane, X = Cl, CH3O, CN, NO). The $S = {}^1/_2$ reversible arrow $S = {}^3/_2$ spin equilibrium of [FeLPr(NO)], *Inorg. Chem. 41*, 3444−3456.
33. Silaghi-Dumitrescu, I. (2004) Ph.D. Thesis, Department of Chemistry, University of Georgia, Athens, GA.
34. Jin, S., Kurtz, D. M., Jr., Liu, Z.-J., Rose, J., and Wang, B.-C. (2002) X-ray crystal structures of reduced rubrerythrin and its azide adduct: a structure-based mechanism for a non-heme diiron peroxidase, *J. Am. Chem. Soc. 124*, 9845−9855.
35. Voegtli, W. C., Sommerhalter, M., Saleh, L., Baldwin, J., Bollinger, J. M., and Rosenzweig, A. C. (2003) Variable coordination geometries at the diiron(II) active site of ribonucleotide reductase R2, *J. Am. Chem. Soc. 125*, 15822−15830.
36. Haskin, C. J., Ravi, N., Lynch, J. B., Münck, E., and Que, L., Jr. (1995) Reaction of NO with the reduced R2 protein of ribonucleotide reductase from *Escherichia coli*, *Biochemistry 34*, 11090−11098.
37. Coufal, D. E., Tavares, P., Pereira, A. S., Hyunh, B. H., and Lippard, S. J. (1999) Reactions of nitric oxide with the reduced non-heme diiron center of the soluble methane monooxygenase hydroxylase, *Biochemistry 38*, 4504−4513.
38. Whittington, D. A., and Lippard, S. J. (2001) Crystal structures of the soluble methane monooxygenase hydroxylase from *Methylococcus capsulatus* (Bath) demonstrating geometrical variability at the dinuclear iron active site, *J. Am. Chem. Soc. 123*, 827−838.
39. Enemark, J. H., and Feltham, R. D. (1974) Principles of structure, bonding, and reactivity for metal nitrosyl complexes, *Coord. Chem. Rev. 13*, 339−406.
40. Serres, R. G., Grapperhaus, C. A., Bothe, E., Bill, E., Weyhermuller, T., Neese, F., and Wieghardt, K. (2004) Structural, spectroscopic, and computational study of an octahedral, non-heme $\{Fe-NO\}^{6-8}$ series: $[Fe(NO)(cyclam\text{-}ac)]^{2+/+/0}$, *J. Am. Chem. Soc. 126*, 5138−5153.
41. Solomon, E. I., Brunold, T. C., Davis, M. I., Kemsley, J. N., Lee, S.-K., Lehnert, N., Neese, F., Skulan, A. J., Yang, Y.-S., and Zhou, J. (2000) Geometric and electronic structure/function correlations in non-heme iron enzymes, *Chem. Rev. 100*, 235−349.

BI0473049